Scientific Research Publishing

Performance Enhancement of CZTS Solar Cell with CuSbS₂ Back Surface Field: A Numerical Simulation Approach

Md. Ferdous Wahid*, Nowshad Ahmed, Md. Shahriar Rahman, Abdullah Al Mamun, Md. Nuralam Howlader, Md. Motiur Rahman Tareq

Department of Electrical and Electronic Engineering, Hajee Mohammad Danesh Science and Technology University, Dinajpur, Bangladesh
Email: *mfwahid26@gmail.com

Abstract

Copper Zinc Tin Sulfide (CZTS) solar cell (SC) has garnered significant attention from researchers in recent years owing to its affordability, less toxic earth abundant constituents, remarkable conversion efficiency and promising prospects for the bulk manufacture of thin film solar cells. Moreover, CZTS exhibits a high absorption coefficient and possesses an optimal adjustable direct band gap, making it a promising candidate for various photovoltaic applications. Hence, in this study, a new configuration (CuSbS₂/CZTS/CdS/i-ZnO/Al: ZnO) is introduced for CZTS SC, which was simulated using SCAPS-1D. The utilization of CuSbS₂ as the back surface field (BSF) and CdS as the buffer layer was investigated to enhance the performance of CZTS SC. Moreover, a comparative numerical analysis was carried out to contrast the SC configurations of CZTS/CdS/i-ZnO/Al: ZnO and CuSbS₂/CZTS/CdS/i-ZnO/Al: ZnO. In this study, the impact on SC parameters such as open circuit voltage (V_{oc}), short-circuit current density (J_{sc}), Fill-factor (FF), and Power Conversion Efficiency (PCE) by varying thickness, doping density, defect density of absorber and buffer layer, thickness and doping density of BSF, and operating temperature have been thoroughly investigated. The optimum structure consists of i-ZnO and Al: ZnO for the window layer, CdS for the buffer layer, CZTS for the absorber layer, and BSF layers with thicknesses of 50 nm, 200 nm, 50 nm, 2000 nm, and 50 nm, respectively. The designed SC with a BSF layer had a PCE of 28.76%, J_{SC} of 32.53 mA/cm², V_{oc} of 1.01233 V, and FF of 87.35%. The structure without a BSF layer has a PCE of 24.21%, V_{oc} of 0.898 V, J_{SC} of 31.56 mA/cm², and FF of 85.32%. Furthermore, an analysis of temperature, quantum efficiency (QE), C-V characteristics and the J-V curve was conducted, revealing the potential of

CuSbS$_2$ as a BSF and CdS as a buffer layer in high-performance, cost-effective CZTS SC designs.

Keywords

Solar Cell, CZTS, BSF, Defect Density, Doping Concentration, SCAPS-1D

1. Introduction

Traditional energy sources that include coal, fossil fuels, natural gas, etc., have detrimental effects on human civilization and the environment [1]. Research efforts are therefore focused on finding and developing alternative sources of energy to address long-term energy needs while minimizing negative impacts on the economy and environment. Solar energy, being a renewable resource with an inexhaustible supply, exhibits significant potential to meet daily energy needs. In addition, solar energy is inexpensive, and the establishment of more efficient solar cells in recent years has demonstrated enormous potential [2]. CZTS, a kesterite and stannite structured material, has been extensively utilized as one of the most widely adopted SC materials in endeavors to enhance SC efficiency. CZTS solar cells are attractive to researchers due to their low cost, non-toxicity, and bounty of core elements in nature. CZTS has a direct band gap energy of about 1.4 eV to 1.5 eV and an optical absorption coefficient of 10^4 cm^{-1}. The cheapness of CZTS materials and their high melting point (990°C) indicate their potential for practical manufacture using an affordable solution technique, hence ensuring long-term operational durability [3] [4] [5] [6]. Spin-coating and sputtering processes are commonly used for CZTS SC fabrication. Nevertheless, the CZTS material exhibits certain limitations, with its primary drawback being the disorder of Cu-Zn cations, leading to a substantial deficit in the V$_{OC}$ due to electron trapping. However, temperature treatment can overcome this limitation significantly.

Several novel investigations have already been undertaken to explore the efficacy of CZTS solar cells. Cadmium sulfide (CdS), zinc selenide (ZnSe), and indium sulfide (In$_2$S$_3$) are commonly employed as buffer layers in conjunction with CZTS as the absorber layer in thin film solar cells [7] [8]. However, the Shockley-Queisser limit states that the optimal conversion efficiency for CZTS solar cells is 32.2% [9]. A research investigation successfully attained an efficiency of 18.66% with a 2000 nm thick CZTS absorber layer and a 100 nm thick CdS buffer layer [10]. Additionally, a different approach obtained 18.68% efficiency by employing FTO as the window layer, In$_2$S$_3$ as the buffer layer, CZTS as the absorber layer and Mo as back contact [11], while another study on CZTS SC recorded 19.23% efficiency with a ZnO window layer, a 50 nm thick In$_2$S$_3$ buffer layer, and a 1000 nm thick CZTS absorber layer [12]. A photovoltaic device composed of the Al-ZnO/CdS/CZTS/MoO$_3$/Au structure achieved a PCE of 22.28% during an in-

vestigation into the utilization of MoO_3 as the back-surface field. The enhanced efficiency observed in this case can be attributed to the utilization of MoO_3 BSF, which effectively facilitates carrier transportation, promotes their accumulation at the electrodes, and minimizes carrier recombination at the interface [9]. Hence, it is imperative to consider the implementation of a BSF layer with the intention of enhancing the performance of conventional CZTS SCs. These developments signify promising progress in the utilization of CZTS solar cells for improved energy conversion and renewable energy applications.

In this paper, a comprehensive investigation of proposed CZTS-based SCs performance parameters with and without $CuSbS_2$ BSF was carried out employing SCAPS 1D simulation software. The investigation was conducted to inspect the impact of various factors, including the thickness, doping density, and defect density of the absorber and buffer layer, as well as the thickness and doping density of the back surface field (BSF), and the operating temperature, on the output parameters of a solar cell. The objective of this investigation was to optimize the device structure to enhance photo conversion efficiency.

## 2. Device Configuration and Material Parameters

The numerical analysis of the SC was conducted utilizing SCAPS-1D software specifically designed for SC analysis. This software has been programmed by the esteemed Department of Electronics and Information Systems at the University of Gent, Belgium [13]. The structure may incorporate a maximum of seven distinct layers, six interface layers and two electrodes. SCAPS 1D is a software tool that effectively models and presents an extensive array of parameters related to renewable energy. These parameters encompass crucial aspects such as PCE, FF, V_{oc}, J_{sc}, QE, and J-V characteristics. This software utilizes the Poisson equation, continuity equation, and current density equation to accurately simulate and analyze the various parameters [14]. The schematic representations of CZTS- based SC are visually depicted in **Figure 1**, showcasing the intricate structures. Additionally, the energy band diagram of these structures is thoughtfully illustrated in **Figure 2**, providing a comprehensive understanding of the energy dynamics.

The window layer incorporated in the aforementioned cell composition comprises the intrinsic zinc oxide (i-ZnO) and aluminium doped zinc oxide (Al: ZnO) layer, which is chosen for its cost-effectiveness and exceptional optical transparency [15].

The chosen buffer and absorber layers for this particular application were CdS and CZTS, respectively. Copper antimony sulfide ($CuSbS_2$) has been carefully selected as the back surface field (BSF) layer due to its exceptional band gap and remarkable optical absorption coefficient [16]. SC performance at 300 K is simulated under 100 mW/cm^2 of incident light, 1 MHz of radiation frequency, and AM 1.5G of the solar spectrum. To keep things straightforward, the impact of resistance is not taken into account. **Table 1** shows the important parameters for the various layers, whereas **Table 2** shows the interface and bulk defect parameters.
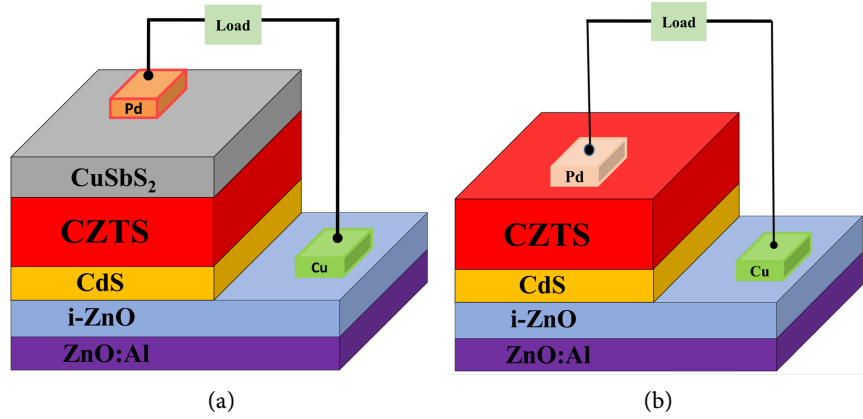
Figure 1. CZTS solar cell configuration (a) with BSF layer (b) without BSF layer.
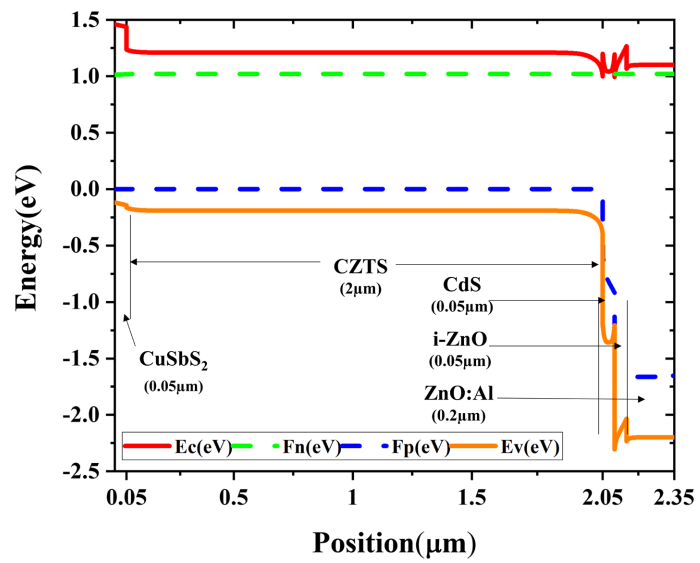
(a)
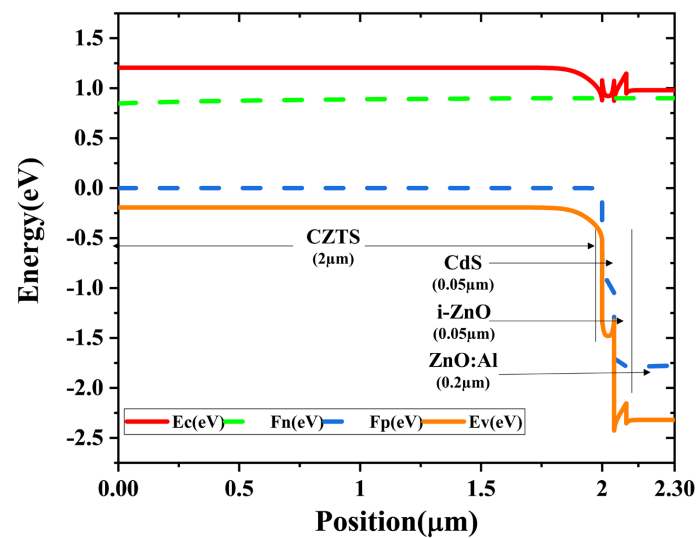
(b)

Figure 2. Energy band diagram (a) with BSF layer (b) without BSF layer.

Table 1. Input parameters that were used in simulation.

Parameters	CuSbS$_2$ [17]	CZTS [18]	CdS [19]	i-ZnO [20]	ZnO: Al [20]
Thickness (nm)	50 - 500	100 - 3000	50 - 500	50	200
Band gap (eV)	1.58	1.4	2.4	3.3	3.3
Electron affinity (eV)	4.2	4.4	4.2	4.4	4.6
Dielectric permittivity (er)	14.6	10	10	7.8	7.8
CB effective DOS (cm^{-3})	2.0×10^{18}	2.2×10^{18}	2.2×10^{18}	2.2×10^{18}	2.2×10^{18}
VB effective DOS (cm^{-3})	1.0×10^{18}	1.8×10^{19}	1.8×10^{19}	1.8×10^{19}	1.8×10^{19}
Electron mobility (cm$^2\cdot$Vs^{-1})	49	100	100	160	160
Hole mobility (cm$^2\cdot$Vs^{-1})	49	25	25	40	40
Donor density (cm^{-3})	0	0	1×10^{12} - 1×10^{18}	1×10^{15}	1×10^{20}
Acceptor density (cm^{-3})	1×10^{12} - 1×10^{18}	1×10^{12} - 1×10^{18}	0	0	0
Defect density (cm^{-3})	1×10^{14}	1×10^{14}	1×10^{14}	1×10^{14}	1×10^{14}

**Table 2.** Bulk and interface defect used in simulation [21].

Parameter	I-ZnO/ZnO: Al Interface	CdS//i-ZnO Interface	CZTS/CdS Interface	CuSbS$_2$/CZTS Interface	Bulk CZTS
Defect type	neutral	neutral	neutral	neutral	neutral
Total defect density (cm^{-3})	1×10^{11}	1×10^{11}	1×10^{11}	1×10^{11}	1×10^{14}
Electron capture cross section (cm^2)	1×10^{-19}	1×10^{-19}	1×10^{-19}	1×10^{-19}	1×10^{-15}
Hole capture cross section (cm^2)	1×10^{-19}	1×10^{-19}	1×10^{-19}	1×10^{-19}	1×10^{-15}
Energy distribution	single	single	single	single	single
Reference defect energy level	0.6	0.6	0.6	0.6	0.6

3. Results and Discussion

3.1. Impact of Absorber Layer Thickness and Doping Density Variation on PV Cell

Figure 3 exemplifies the simultaneous effect of varying the thickness of the absorber layer and acceptor doping (N$_A$) on PV parameters. The thickness and N$_A$ were varied from 0.5 μm to 2.5 μm and 10^{13} cm^{-3} to 10^{19} cm^{-3}, respectively. More photons are absorbed by a thick absorber layer, which also produces many electron-hole pairs [22]. Consequently, J$_{sc}$ rises from 28.78 mA/cm^2 at 0.5 μm CuSbS$_2$ absorber layer thickness to 31.72 mA/cm^2 at 1 μm, as shown in **Figure 3(b)**. The effect of increasing the thickness of the absorber layer from 0.5 μm to 2.5 μm is seen in **Figure 3(a)**, where V$_{oc}$ marginally decreases from 1.039 V to 0.9750 V while recombination rises with the thickness of the absorber layer. V$_{oc}$ and J$_{sc}$, on the contrary, displayed a reversed characteristic for rising doping density. According to **Figure 3(a)** and **Figure 3(b)**, the greatest V$_{oc}$ and J$_{sc}$ values were 1.233

V and 29.76 mA/cm² at N_A 10^{20} cm⁻³, respectively. The excessive absorption of free carriers, which rises linearly along with the number of carriers, might be blamed for the decrease in short circuit current at greater doping concentrations [23]. **Figure 3(c)** demonstrates the influence of simultaneous variations in N_A and thickness on the Fill Factor (FF). The greatest FF was achieved when the N_A was 10^{-19} cm⁻³ and the thickness was 0.5 μm. The range of FF from 82.88% to 89.65% was observed when the N_A was greater than 10^{15} cm⁻³ and the thickness was between 0.5 μm and 2.5 μm. Similarly, FF was obtained ranging 80.35% to 81.51% when N_A was less than 10^{15} cm⁻³ and thickness was equaled or surpassed 1.5 μm. Additionally, FF was more affected by the variation of N_A. **Figure 3(d)** shows the impact on PCE due to varying N_A and thickness simultaneously. When the N_A is less than 10^{19} cm⁻³ and the thickness is between 0.5 μm to 2.5 μm, the PCE is achieved from 28.58% to 32.14%. It was found that PCE was less affected by thickness variations. When thickness was altered from 1 μm to 2.5 μm and N_A was above 10^{18} cm⁻³, the maximum PCE was achieved from about 33.23% to 34.32%. The maximum value of PCE was obtained when N_A was 10^{19} cm⁻³ and thickness was 2 μm. Therefore, the thickness and acceptor doping density both exert a substantial implication on the solar cell's overall performance. In this study, the optimal thickness and the absorber doping density of absorber layer were kept at 2 μm and 1×10^{18} cm⁻³ considering the structure size and fabrication cost for further optimization.
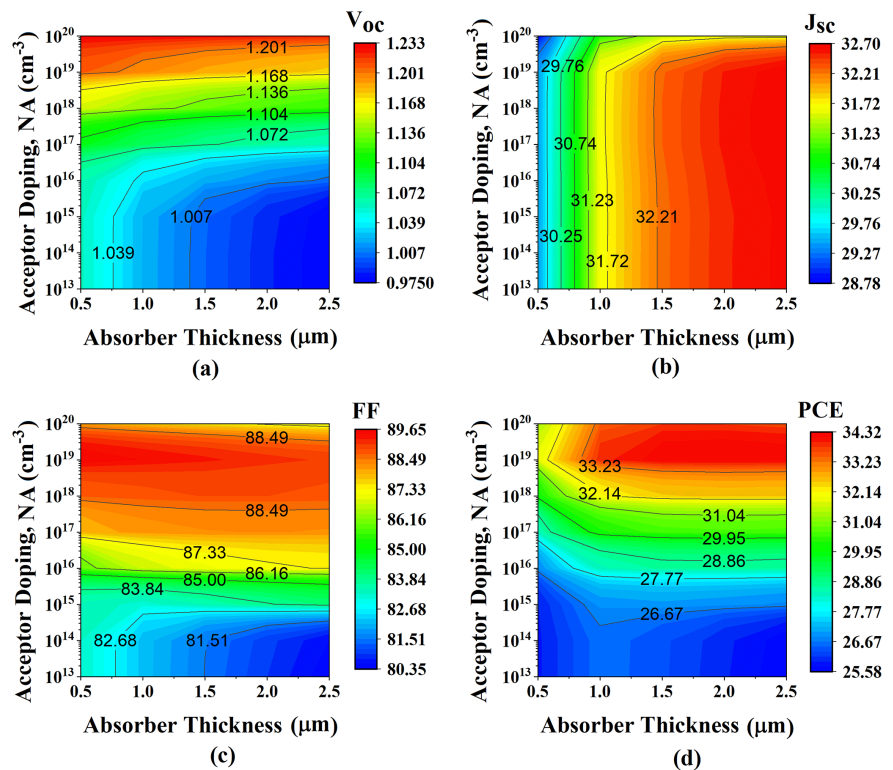
Figure 3. Contour plot visualization of the effect on PV parameters with the variation of thickness and doping density.

3.2. Impact of Absorber Defect Density on PV Cell

Figure 4 depicts the effect of defect density of the absorber layer with and without the BSF layer. The defect density was varied from 10^{10} to 10^{16} cm^{-3} in both structures. All PV parameters were stable up to a defect density of 10^{15} cm^{-3}. When the defect density rises above that limit, a reduction in all parameters is observed. With the BSF layer, the V_{oc}, J_{sc}, FF, and PCE all dropped from 1.06 V to 0.94 V, 32.45 mA/cm^2 to 31.29 mA/cm^2, 86.45% to 82.86%, and 28.85% to 22.87%, respectively. The structure without the BSF had similar effects, but the range of reduction was different. V_{oc} drops from 0.897 to 0.874 V, J_{sc} from 32.45 mA/cm^2 to 31.29 mA/cm^2, FF from 85.43% to 81.83%, and PCE from 24.25% to 22.39% at the same range of variation. Because electron-hole pair formation is hindered by an excessive defect level, J_{sc} decreases as defect density increases. Additionally, the process of Shockley-Read-Hall (SRH) carrier recombination causes a decline in V_{oc} with an improvement in the dark current [22] [23] [24] [25]. Therefore, the optimal value of defect density was set to 10^{14} cm^{-3}.

3.3. Impact of Buffer Layer Thickness, Doping and Defect Density on Solar Cell

A solar cell's buffer layer is essential for eliminating electrons and holes from both sides of the cell's structure. A better electron-hole pair formation is achieved by increased photon absorption when a larger band gap buffer substance is utilized instead of the absorber material to transmit incoming light to the junction
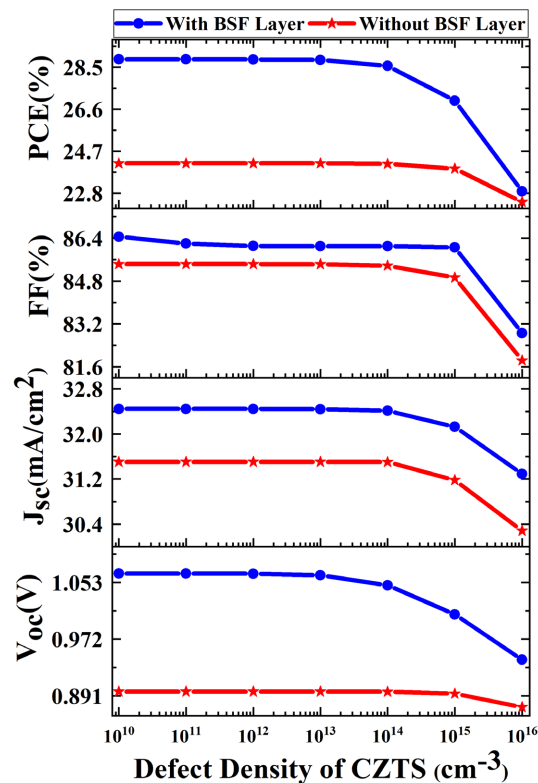

**Figure 4.** Defect density variation of CZTS absorber layer.

region. Additionally, an effective gathering of carriers produced by photons was provided by the controlled carrier (electron) flow from the photo-active area of the cell to the exterior metal electrode (front contact) [20]. To enable the most incoming light to pass easily a thickness that is as thin as feasible is needed. However, a very thin thickness might result in an audible leakage current [26]. **Figure 5(a)** shows how changing the thickness of the buffer layer (CdS) affects the PV parameters with and without the BSF layer. The thickness of buffer layers ranged from 0.01 μm to 0.1 μm. Changes in thickness had no effect on PV parameters for either case with or without the BSF layer due to the thick absorber layer. The structure including the BSF layer performs better than the other one. **Figure 5(b)** shows that the V_{oc} curve remains nearly the same for both with and without the BSF layer at 1.01 V and 0.90 V when the doping concentration of the CdS layer is increased from 10^{12} cm^{-3} to 10^{19} cm^{-3}. In the presence of a BSF layer, J_{sc} is 32.54 mA/cm^2 regardless of doping concentration. The J_{sc} value stays at 31.14 mA/cm^2 till a doping density of 10^{16} without the BSF layer. Beyond this point, the J_{sc} steadily increases with increased doping density until it hits a saturation point at roughly 31.5 mA/cm^2 at 10^{17} cm^{-3} doping density. The fill factor of the two structures with and without the BSF layer remains around 85.30% and 67.30%, respectively, up to a doping concentration of 10^{14} cm^{-3}, after which the FF of the structure without BSF layer gradually rises to a maximum value of 85.41% as the doping density increases. The structure with the BSF layer, on the other hand, exhibits a slight boost in the FF after doping concentration 10^{14} cm^{-3}, with a maximum value of 87.37%. Similar to FF, PCE has a similar behavior, with values remaining nearly constant until 10^{14} for both the presence of the BSF layer and the case without the BSF. Thereafter, further increasing the doping density causes the PCE to increase to maximum values of 28.74% and 24.17%, respectively. **Figure 5(c)** illustrates the repercussions of the defect density of the buffer layer on the PV parameters, both in the presence and absence of the BSF layer. The range of defect density observed was between 10^{10} cm^{-3} and 10^{16} cm^{-3}. The observed variations in defect density did not have discernible effects on the PV characteristics, regardless of the presence or absence of the BSF layer. Due to its smaller thickness, concentration, and high bandgap which was demonstrated in prior research, CdS buffer layer defect density has a negligible impact on performance parameters [20]. Hence, it can be inferred that the implementation of the BSF layer enables the achievement of improved PV parameters at a lower doping density of the buffer layer. In its absence, even with higher doping concentration, comparable performance remains unattainable. The optimum thickness, doping density, and defect density were therefore adjusted to 50 nm, 10^{18} cm^{-3}, and 10^{14} cm^{-3}, respectively.
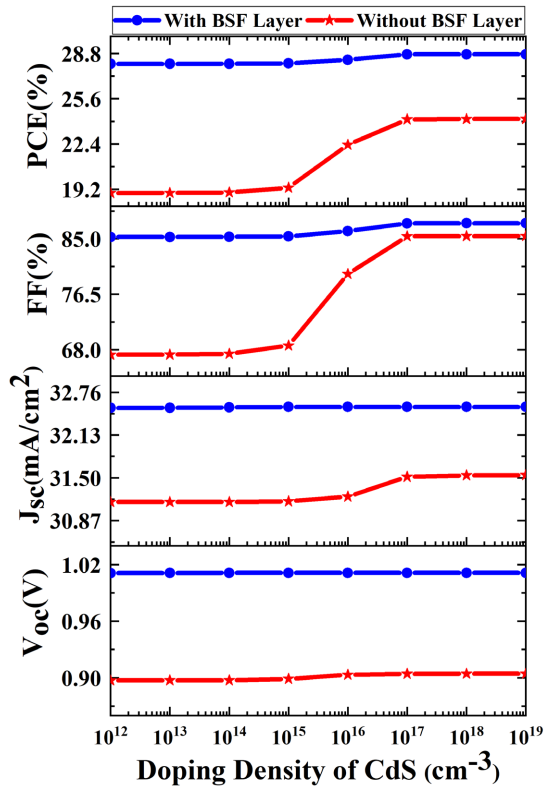
3.4. Impact of BSF Layer Thickness and Doping Density on Solar Cell

The effect of CuSbS$_2$ BSF thickness and doping concentration on device performance has been investigated in **Figure 6(a)** and **Figure 6(b)** noticeably
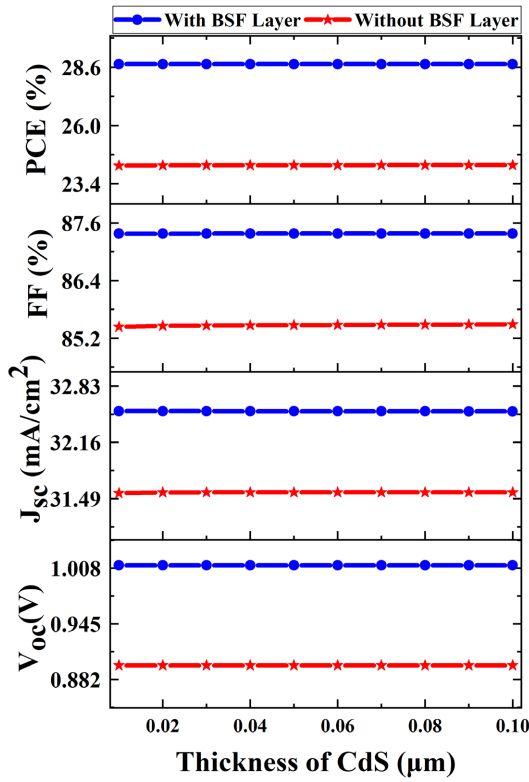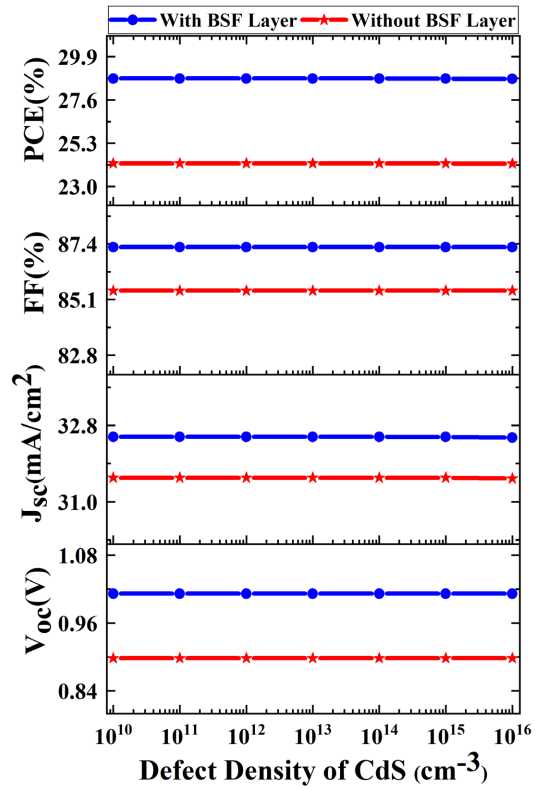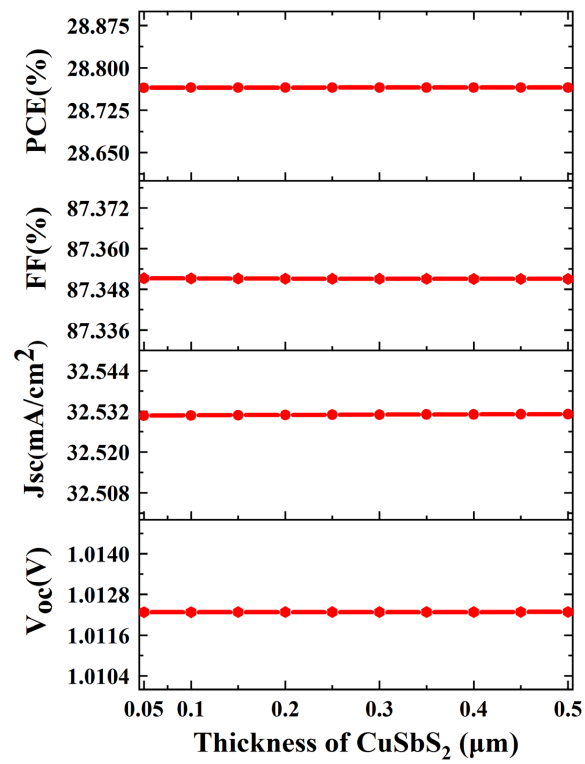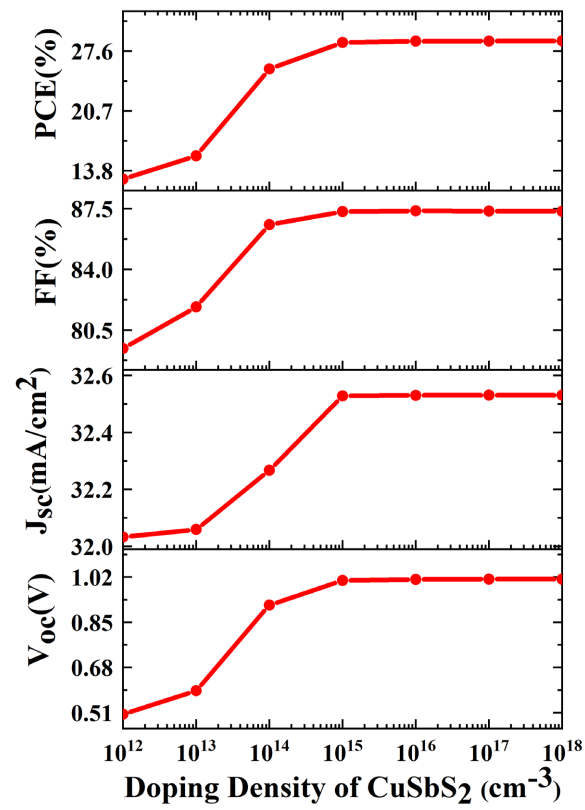
(a)

(b)

(c)

Figure 5. Variation of (a) thickness (b) doping concentration and (c) defect density of buffer layer with and without BSF layer and its effect on PV parameters.

(a)

(b)

Figure 6. Variation of (a) thickness and (b) doping concentration of BSF layer and its effect on PV parameters.

demonstrates that all the PV parameters remained steady in relation to the thickness of BSF. There could be no denying that infected absorption rises as BSF layer thickness is enhanced [27]. The simulation shows that, increasing the thickness of the BSF layer could not contribute to increasing the built-in- potential at the interface in the structure. However, all the PV parameters showed significant variation based on doping concentration. With the increase of doping concentration from 10^{12} to 10^{18} cm^{-3}, V_{oc} was increased from 0.503 to 1.012 V, J_{sc} from 32.03 mA/cm^2 to 32.53 mA/cm^2, FF from 79.43% to 87.35%, and efficiency from 12.82% to 28.74%. It is found that all the parameters rose rapidly up to a doping density of 10^{15} cm^{-3} after that it became almost saturated. The enhancement might be caused by the impact of adding additional dopants, which increases the concentration of free carriers and acceptors, which reduces the interdiffusion of grains inside the BSF layer and passivates flaws [28]. Further increase in doping retained almost the same result of parameters. Therefore, the optimal value of thickness and doping density was determined at 0.05 μm and 10^{15} cm^{-3} to reduce fabrication cost.

3.5. Effect of Temperature Variation

The detrimental effect of operational temperature from 270 K to 330 K on performance parameters is shown in Figure 7. According to simulation, V_{oc}, FF,
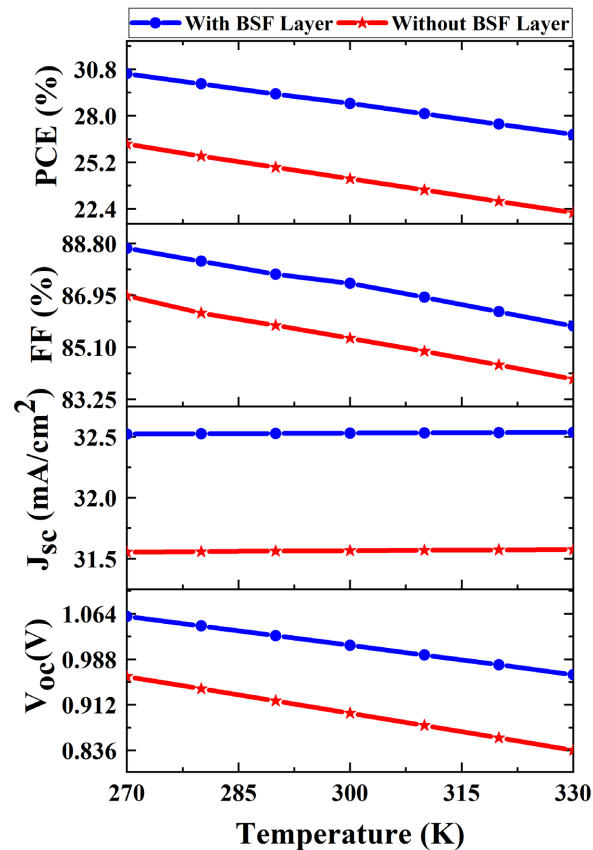

**Figure 7.** Variation of temperature and its effect on PV parameters.

and PCE decreased as temperature increased, whereas J_{sc} nearly remained constant for the recommended structure with as well as without BSF. At 270 K and 330 K, the efficiency of the cell without a BSF layer was found to be 26.30% and 22.17%, respectively, while the PCE of the suggested SC with a BSF layer ranged from 30.54% to 26.88% over the same temperature range. These simulation results show that a CZTS SC with a BSF layer can have better thermal stability than a device without a BSF layer. Similar findings have been observed in previous studies [19].
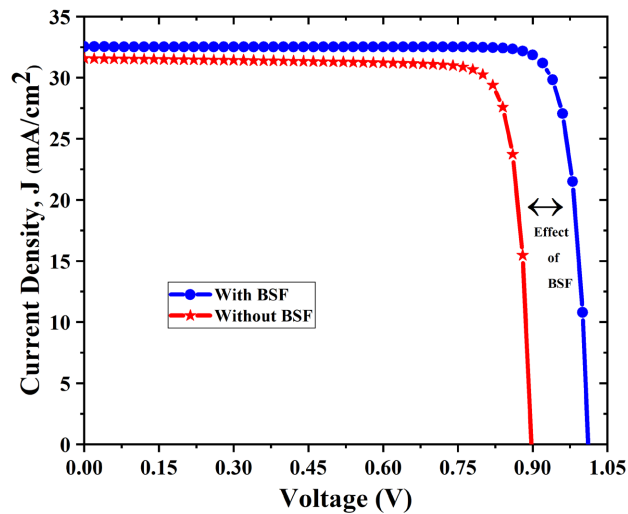
3.6. C-V Characteristics Curve

Figure 8 depicts the correlation between capacitance and applied voltage within the specified range of −0.8 V to 0.8 V for the configuration that includes a back surface field (BSF) layer. The experiment was carried out at a frequency of 1 MHz to mitigate the impact of deep level traps. The image provided demonstrates that an enhancement in the supply voltage results in a significant exponential expansion in capacitance. The figure exhibits a non-linear shape as a result of the presence of several junctions. However, it can be deduced that the device reaches the depletion region when the bias is adjusted to a value of zero. The implementation of forward bias leads to a notable growth in capacitance. The utilization of reverse bias results in a significant decrease in capacitance.

### 3.7. Impact of J-V & QE Characteristics

Figure 9(a) demonstrates the J-V characteristics of CZTS SC with the presence of a BSF layer and without the BSF layer. It is observed from the Figure that CZTS SC without BSF layer produced a PCE of 24.23% with J_{sc} of 31.56 mA/cm², V_{oc} of 0.8980 V, and an FF of 85.47%, whereas the addition of BSF layer produced PCE of 28.74% with J_{sc} of 32.53 mA/cm², a V_{oc} of 1.0123 V, and FF of 87.27%. That means, the PV parameters determined by numerical simulation of the SC containing $CuSbS_2$ are significantly greater than the structure without BSF. The improvement in the parameters due to the addition if the BSF layer is
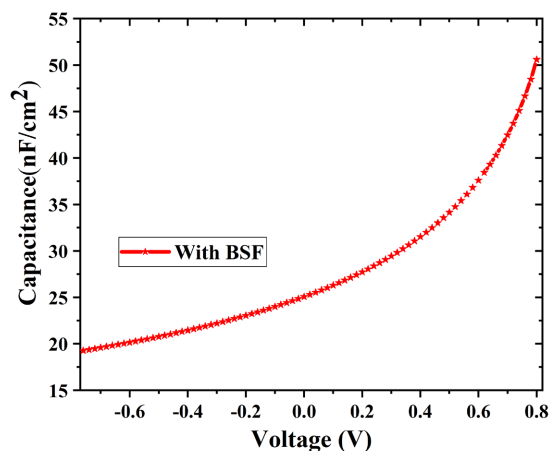
Figure 8. Capacitance vs voltage curve.
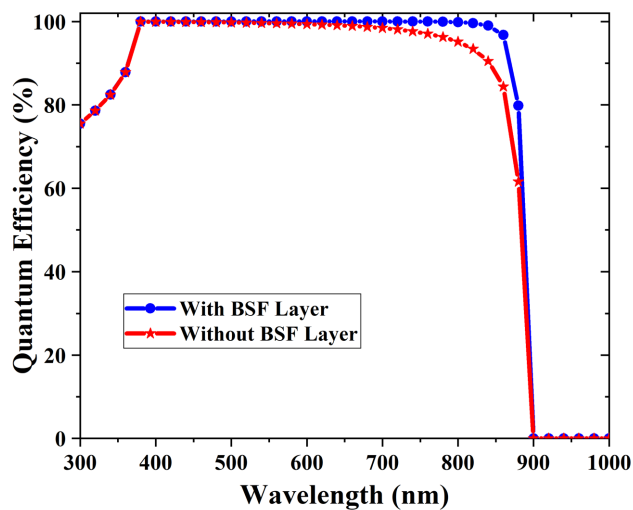
Figure 9. (a) J-V characteristic curve and (b) QE curve.

already identical with the previous research works [29]. The quantum efficiency of the recommended structure with and without BSF has been demonstrated in **Figure 9(b)**. The visible light spectrum is mostly covered by both structures but the recommended solar cell with BSF layer has showed higher performance compared to that of without BSF. This is because of enhancement in absorption due to the inclusion of BSF layer. The similar tendency of QE has already been reported in the previous studies [2].

3.8. Output of SC Parameters

A comprehensive analysis and summary of previous research work on CZTS solar cell architectures are presented in **Table 3**. The numerical simulation of CZTS SC used CuSbS$_2$ as the BSF layer showed improved SC performance over earlier research.

Table 3. Performance evaluation for existing PSCs based on CZTS.

Device	V_{oc} (V)	J_{sc} (mA/cm²)	FF (%)	PCE (%)	References
CuSbS$_2$/CZTS/CdS/i-ZnO/Al: ZnO	1.0123	32.53	87.35	28.76	This work
CZTS/CdS/i-ZnO/Al: ZnO	0.898	31.56	85.32	24.21	This work
Al: ZnO/i-ZnO/ZnSe/CZTS/Se	1.1066	25.84	88.47	25.30	[8]
n-ZnS/p-CZTS/p⁺-WSe$_2$	0.96	33.72	83.75	27.31	[30]
FTO/In$_2$S$_3$/CZTS/Mo	0.8787	25.258	84.17	18.68	[11]

This research has explored the potential benefits of combining CZTS SC with a BSF layer made of CuSbS$_2$. The CuSbS$_2$ BSF layer facilitates carrier transportation, promotes their accumulation at the electrodes, and minimises carrier recombination at the interface which in turns, enhancing the performance of PV parameters.

4. Conclusion

This research work employed SCAPS-1D software to numerically analyze the impact of the CuSbS$_2$ BSF layer on the PV parameters of CZTS solar cell. During the simulation, the impacts of thickness, defect density, doping concentration, quantum efficiency, and temperature on solar cell output parameters are studied. Incorporating CuSbS$_2$ as a BSF layer led to a PCE of 28.76%, V_{oc} of 1.0123 V, J_{sc} of 32.53 mA/cm², and FF of 87.35%, while without BSF layer-based CZTS structure yielded a PCE of 24.21%, V_{oc} of 0.898 V, J_{sc} of 31.56 mA/cm², and FF of 85.32%. This implies that the overall performance of the SC is greatly improved by using CuSbS$_2$ as the BSF layer. The optimized structure yielded the highest efficiency for CZTS, CdS, and CuSbS$_2$ layer thicknesses of 2 μm, 0.05 μm, and 0.05 μm with carrier concentrations of 1×10^{16} cm^{-3}, 1×10^{18} cm^{-3}, and 1×10^{18} cm^{-3} at 300 K. This numerical simulation shows that CZTS-based thin film solar cells can perform better with an appropriate BSF layer.

Acknowledgements

Conflicts of Interest

The authors declare no conflicts of interest regarding the publication of this paper.

References

[1] Tang, H., He, S. and Peng, C. (2017) A Short Progress Report on High-Efficiency Perovskite Solar Cells. *Nanoscale Research Letters*, **12**, Article No. 410.

https://doi.org/10.1186/s11671-017-2187-5

[2] Ali, M.H., Al Mamun, M.A., Haque, M.D., Rahman, M.F., Hossain, M.K. and Md. Touhidul Islam, A.Z. (2023) Performance Enhancement of an MoS_2-Based Heterojunction Solar Cell with an In_2Te_3 Back Surface Field: A Numerical Simulation Approach. *ACS Omega*, **8**, 7017-7029. https://doi.org/10.1021/acsomega.2c07846

[3] Arnous, A.H., Biswas, A., Ekici, M., Alzahrani, A.K. and Belic, M.R. (2021) Optical Solitons and Conservation Laws of Kudryashov's Equation with Improved Modified Extended Tanh-Function. *Optik* (*Stuttg*), **225**, Article ID: 165406. https://doi.org/10.1016/j.ijleo.2020.165406

[4] Moghadam, P.K. and Hayati, M. (2019) A Novel Design of Double Junction CZTS/CdS Solar Cell with Transparent Intermediate Layer. *Optik* (*Stuttg*), **194**, Article ID: 163059. https://doi.org/10.1016/j.ijleo.2019.163059

[5] Crovetto, A. and Hansen, O. (2017) What Is the Band Alignment of $Cu_2ZnSn(S,Se)_4$ Solar Cells? *Solar Energy Materials and Solar Cells*, **169**, 177-194. https://doi.org/10.1016/j.solmat.2017.05.008

[6] Tripathi, S., Kumar, B. and Dwivedi, D.K. (2020) Study on Formation and Characterization of Kesterite CZTSSe Thin Films Deposited by Thermal Evaporation Technique for Solar Cell Applications. *Journal of Materials Science: Materials in Electronics*, **31**, 8308-8315. https://doi.org/10.1007/s10854-020-03366-y

[7] Houimi, A., Gezgin, S.Y., Mercimek, B. and Kılıç, H.Ş. (2021) Numerical Analysis of CZTS/n-Si Solar Cells Using SCAPS-1D. A Comparative Study between Experimental and Calculated Outputs. *Optical Materials* (*Amst*), **121**, Article ID: 111544. https://doi.org/10.1016/j.optmat.2021.111544

[8] Talukder, D., Pal, R., Hasan, M.N. and Wahid, M.F. (2021) Numerical Simulation of CZTS Solar Cell with ZnSe Buffer Layer. 2021 *International Conference on Automation, Control and Mechatronics for Industry* 4.0 (*ACMI*), Rajshahi, 8-9 July 2021, 1-6. https://doi.org/10.1109/ACMI53878.2021.9528287

[9] Ait Abdelkadir, A. and Sahal, M. (2023) Theoretical Development of the CZTS Thin-Film Solar Cell by SCAPS-1D Software Based on Experimental Work. *Materials Science and Engineering: B*, **296**, Article ID: 116710. https://doi.org/10.1016/j.mseb.2023.116710

[10] Paswan, S.K., Chandra, D., Bhatt, U.M. and Kumar, B. (2020) Performance Enhancement of CZTS and CZTSSe Solar Cells Using CdS as Buffer Layer. 2020 *International Conference on Electrical and Electronics Engineering* (*ICE*3), Gorakhpur, 14-15 February 2020, 728-732. https://doi.org/10.1109/ICE348803.2020.9122898

[11] Shahid, A., Daud Khan, A. and Ur Rehman, O. (2019) Modelling of Highly Efficient Copper Zinc Tin Sulphide (CZTS) Solar Cell for Performance Improvement. 2019 *International Conference on Electrical, Communication, and Computer Engineering* (*ICECCE*), Swat, 24-25 July 2019, 1-5. https://doi.org/10.1109/ICECCE47252.2019.8940765

[12] Mohammad, S., Tousif, M.N., Ferdous, A.A., Hoque, M.A. and Rahman, M.W. (2017) Numerical Analysis of CZTS Solar Cell with In_2S_3 Buffer Layer: A Study of a CZTS Based Thin Film Solar Cell, Concerning the Effects of Several Parameters on Its Electrical Performance. 2017 *IEEE International Conference on Smart Grid and Smart Cities* (*ICSGSC*), Singapore, 23-26 July 2017, 55-60. https://doi.org/10.1109/ICSGSC.2017.8038549

[13] Zaidi, B., Zouagri, M., Merad, S., Shekhar, C., Hadjoudja, B. and Chouial, B. (2019) Boosting Electrical Performance of CIGS Solar Cells: Buffer Layer Effect. *Acta Phy-*

sica Polonica A, **136**, 988-991. https://doi.org/10.12693/APhysPolA.136.988

[14] Burgelman, M., Nollet, P. and Degrave, S. (2000) Modelling Polycrystalline Semiconductor Solar Cells. *Thin Solid Films*, **361**-**362**, 527-532.
https://doi.org/10.1016/S0040-6090(99)00825-1

[15] Hedibi, A., Gueddim, A. and Bentria, B. (2021) Numerical Modeling and Optimization of ZnO:Al/i-ZnO/ZnMgO/CZTS Photovoltaic Solar Cell. *Transactions on Electrical and Electronic Materials*, **22**, 666-672.
https://doi.org/10.1007/s42341-020-00278-w

[16] Touati, R., Ben Rabeh, M. and Kanzari, M. (2014) Structural and Optical Properties of the New Absorber Cu_2ZnSnS_4 Thin Films Grown by Vacuum Evaporation Method. *Energy Procedia*, **44**, 44-51. https://doi.org/10.1016/j.egypro.2013.12.008

[17] Deepthi Jayan, K. (2021) Enhancement of Efficiency of $(FA)_2BiCuI_6$ Based Perovskite Solar Cells with Inorganic Transport Layers. *Optical Materials* (*Amst*), **122**, Article ID: 111671. https://doi.org/10.1016/j.optmat.2021.111671

[18] Çetinkaya, S. (2019) Study of Electrical Effect of Transition-Metal Dichalcogenide-MoS_2 Layer on the Performance Characteristic of Cu_2ZnSnS_4 Based Solar Cells Using wxAMPS. *Optik* (*Stuttg*), **181**, 627-638.
https://doi.org/10.1016/j.ijleo.2018.12.122

[19] Haque, M.D., Ali, M.H., Rahman, M.F. and Islam, A.Z.M.T. (2022) Numerical Analysis for the Efficiency Enhancement of MoS_2 Solar Cell: A Simulation Approach by SCAPS-1D. *Optical Materials* (*Amst*), **131**, Article ID: 112678.
https://doi.org/10.1016/j.optmat.2022.112678

[20] Isha, A., *et al.* (2023) High Efficiency Cu_2MnSnS_4 Thin Film Solar Cells with SnS BSF and CdS ETL Layers: A Numerical Simulation. *Heliyon*, **9**, e15716.
https://doi.org/10.1016/j.heliyon.2023.e15716

[21] Basyoni, M.S.S., *et al.* (2021) On the Investigation of Interface Defects of Solar Cells: Lead-Based vs Lead-Free Perovskite. *IEEE Access*, **9**, 130221-130232.
https://doi.org/10.1109/ACCESS.2021.3114383

[22] Saha, B., Mondal, B.K., Mostaque, S.K., Hossain, M. and Hossain, J. (2023) Numerical Modeling of $CuSbSe_2$-Based Dual-Heterojunction Thin Film Solar Cell with CIGS Back Surface Layer. *AIP Advances*, **13**, Article ID: 025255.
https://doi.org/10.1063/5.0133889

[23] Guarracino, I., Mellor, A., Ekins-Daukes, N.J. and Markides, C.N. (2016) Dynamic Coupled Thermal-and-Electrical Modelling of Sheet-and-Tube Hybrid Photovoltaic/Thermal (PVT) Collectors. *Applied Thermal Engineering*, **101**, 778-795.
https://doi.org/10.1016/j.applthermaleng.2016.02.056

[24] Alam, I., Mollick, R. and Ashraf, M.A. (2021) Numerical Simulation of $Cs_2AgBiBr_6$-Based Perovskite Solar Cell with ZnO Nanorod and P3HT as the Charge Transport Layers. *Physical Review B—Condensed Matter*, **618**, Article ID: 413187.
https://doi.org/10.1016/j.physb.2021.413187

[25] Boumaour, M., Sali, S., Kermadi, S., Zougar, L., Bahfir, A. and Chaieb, Z. (2019) High Efficiency Silicon Solar Cells with Back ZnTe Layer Hosting IPV Effect: A Numerical Case Study. *Journal of Taibah University for Science*, **13**, 696-703.
https://doi.org/10.1080/16583655.2019.1623476

[26] Lee, J., *et al.* (2021) Atomic Layer Deposition of Ultrathin ZnO Films for Hybrid Window Layers for $Cu(In_x,Ga_{1-x})Se_2$ Solar Cells. *Nanomaterials*, **11**, Article No. 2779. https://doi.org/10.3390/nano11112779

[27] Lu, M., Bowden, S., Das, U. and Birkmire, R. (2007) Interdigitated Back Contact Silicon Heterojunction Solar Cell and the Effect of Front Surface Passivation. *Ap-*

plied *Physics Letters*, **91**, Article ID: 063507. https://doi.org/10.1063/1.2768635

[28] Mbopda Tcheum, G.L., Ngoupo, A.T., Ouédraogo, S., Guirdjebaye, N. and Ndjaka, J.M.B. (2020) Numerical Analysis of Ultrathin Cu(In,Ga)Se$_2$ Solar Cells with Zn(O,S) Buffer Layer. *Pramana*, **94**, Article No. 111. https://doi.org/10.1007/s12043-020-01977-y

[29] Haque, M.D., Ali, M.H. and Islam, A.Z.M.T. (2021) Efficiency Enhancement of WSe$_2$ Heterojunction Solar Cell with CuSCN as a Hole Transport Layer: A Numerical Simulation Approach. *Solar Energy*, **230**, 528-537. https://doi.org/10.1016/j.solener.2021.10.054

[30] Abir, A.T., Joy, A., Mondal, B.K. and Hossain, J. (2023) Numerical Prediction on the Photovoltaic Performance of CZTS-Based Thin Film Solar Cell. *Nano Select*, **4**, 112-122. https://doi.org/10.1002/nano.202200228